PCCP

PAPER

View Article Online
View Journal | View Issue

Cite this: *Phys. Chem. Chem. Phys.*, 2018, **20**, 17927

Dissociative adsorption of O_2 on strained Pt(111)†

Tiantian Xue, Chao Wu,* Xiangdong Ding* and Jun Sun

Received 27th March 2018,
Accepted 11th June 2018

DOI: 10.1039/c8cp01966e

rsc.li/pccp

The adsorption and dissociation of O_2 and the adsorption of O* adatoms over strained Pt(111) surfaces have been systematically studied using density functional theory calculations. When the applied bilateral strain ranges from compressive (−5%) to tensile (5%), the adsorption strengths of O and O_2 at various sites can be varied substantially by 0.3 to 0.9 eV. Moreover, the preferred adsorption site of O_2 also changes from tbt to tfb when tensile strain is larger than 3%. The activation barrier of O_2 dissociation can be significantly varied by nearly 0.4 eV from −3% to 3% strain. Meanwhile, the combination of O* adatoms and the applied strain can pull the Pt atom out of the surface and result in dramatic surface buckling. The *z* direction shift of a Pt atom sandwiched by two fcc O* adatoms is over 0.45 Å when compressive strain goes beyond −2%. The abnormal non-linear responses of O adsorption strength and the lateral O–O interaction to strain all arise from the up-buckled Pt atom. We show that strain is a very powerful tool for tuning the thermodynamic and kinetic properties of oxygen adsorption, dissociation and surface bucking of metal surfaces, which are crucial for understanding the catalytic properties and initial oxidation of transition metal based catalysts.

1. Introduction

Utilizing strain to regulate the activity of heterogeneous catalysts has been exemplified in a variety of single component or alloy metal nanostructures.[1–3] Taking one of the most representative catalysts, Pt, as an example, we can see that the recent advancements of its application are largely in strained form. To illustrate this in a more concrete context, examples of the oxygen reduction reaction (ORR) are invoked. The ORR is a sluggish reaction, but it is of great importance in fuel cells,[4–6] and it is most efficiently catalyzed by Pt based alloys. Li *et al.*[7] synthesized jagged Pt nanowires, which exhibited ultrahigh mass activity for the ORR, nearly doubling the previous records. Their simulations suggested that the surface strain (about −1.8%) in the jagged nanowires played a significant role in enhancing the ORR activity (by decreasing the adsorption strength of adsorbents). Wu *et al.*[8] reported that the ORR activity of icosahedral Pt_3Ni catalysts was about 50% higher than that of the octahedral ones. They found that the tensile strain (average 1.6%) in the former increased the catalytic performance by enhancing the adsorption strength of the key adsorbate OH, while the compressive strain (average −1.6%) in the latter lowered the reactivity.

In the ORR and many other oxidation reactions that involve oxygen, the behaviors of the O_2 molecule and its dissociation product atomic O* adatoms on the Pt surfaces are crucial to understand the whole reaction. O_2 molecules can adsorb onto the Pt(111) surface easily and remain molecularly only at very low temperature (<150 K).[9] Usually, O_2 sits over two Pt atoms in a top–bridge–top fashion (binding energy of −0.65 eV), and it also can tilt over to the pocket formed by three Pt atoms by assuming two less stable configurations: top–fcc–bridge and top–hcp–bridge (binding energy of −0.53 and −0.43 eV, respectively).[10] Higher temperature (>150 K) leads to its dissociation, which has been theoretically confirmed to go through a few pathways with low barriers.[10–12] The direct "stretch" or "rotate-then-stretch" transition states are sensitive to the indirectly contacting Pt atoms in the second and even lower layers.[11,13] The atomic products, O* adatoms, are found to dwell favorably in the three-fold hollow sites, and the adatoms usually perturb the surface atoms.[14] Several papers have shown that chemisorbed O atoms, which induce the surface buckled Pt oxide chain at moderate O coverage, are the initial oxidation stage of the unstrained Pt(111) surface.[9,15–17] Naturally, all these behaviors are highly dependent on the substrates, which are subjected to various generic strains, caused by the shape or size of the nanoparticles, nanowires, *etc.* or due to the lattice mismatch in heterostructures. In fact, Grabow *et al.*[18] have investigated the dissociation of O_2 on strained Pt(111) surfaces and they found that strain (+2% to −4%) evidently affects the energetics of one dissociation pathway. However, how do the other possible pathways

Frontier Institute of Science and Technology, State Key Laboratory for Mechanical Behavior of Materials, Xi'an Jiaotong University, Xi'an 710049, People's Republic of China. E-mail: chaowu@mail.xjtu.edu.cn, dingxd@mail.xjtu.edu.cn

† Electronic supplementary information (ESI) available. See DOI: 10.1039/c8cp01966e

vary over strained surfaces? Which pathway will be more favorable under strain? More importantly, after O_2 dissociation, the surface local environment will be oxygen-rich, so how do the O* adatoms affect the deformation (oxidation) of surface atoms under strain? All these questions call for a comprehensive study of the O_2 dissociation kinetics over a strained Pt surface.

In this paper, we report our systematic study of the strain effects on the O_2/O/Pt(111) system. We focus on the behaviors of both the adsorbates and the surface under biaxial strain ranging from −5% to 5%. We first study the thermodynamic properties of O_2/O on strained Pt surfaces, including adsorption and diffusion. Then, we compare the O_2 dissociation pathways under compressive and tensile strain. Later, we analyze adsorption-induced surface Pt atom buckling as a function of strain. Finally, we summarize the strain effects on adsorbates as well as metal surfaces.

2. Theoretical methods

Density functional theory (DFT) calculations were performed using the Dmol3 program package.[19,20] The generalized gradient approximation (GGA) with the Perdew–Wang-91 (PW91)[21,22] functional was employed to account for the exchange–correlation interaction. The atomic orbital basis set with double-numerical plus d (DND) was used in the expansion of molecular orbitals. The core electrons were treated using DFT Semi-core Pseudopots (DSPP).[23] The Brillouin zone was sampled using Monkhorst–Pack grids of 10 × 10 × 10 and 5 × 5 × 1 for the bulk and slab calculations, respectively. The orbital occupancy thermal smearing was set to 0.005 Ha. The convergence criteria for the maximum energy change, the maximum force and the maximum displacement were set to 10^{-5} Ha, 0.002 Ha Å^{-1} and 0.005 Å, respectively.

The Pt(111) surface was modeled using a four-layer symmetric periodic slab with a supercell size of 3 × 3. A vacuum region of 15 Å was added to diminish the interactions between slab images. A test of a larger supercell with more layers of atoms under strain verified that the current supercell model can afford converged adsorption energies. The calculated lattice constant of Pt was 3.99 Å, which is in great agreement with previous DFT calculations[10,11,24] and also quite close to the experimental value of 3.92 Å. Biaxial strain ranging from −5% to 5% was applied in parallel to the surface by changing the lengths of the surface vectors accordingly. The oxygen species were adsorbed on only one side of each slab. The adsorbates and the upper two layers of the slab were allowed to relax during all of the calculations, while the bottom two layers were frozen at their bulk positions. The equilibrium bond length of O_2 of 1.224 Å agreed well with the experimental value of 1.210 Å.[25] A complete linear synchronous transit and quadratic synchronous transit (LST/QST) method[26,27] was adapted to locate the saddle point roughly, and then the saddle point confirmation and the eigenvector following (EF)[27] methods were employed to make sure that all of the reactions were elementary and every transition state obtained had only one imaginary frequency.

The adsorption strength, *i.e.*, formation energy (E_{form}) of an adsorbed molecule or atom using the slab model was defined by:

$$E_{form} = [E_{adsorbate/slab} - (E_{adsorbate} + E_{slab})]/N \quad (1)$$

where $E_{adsorbate/slab}$ is the total energy of the adsorption system, $E_{adsorbate}$ is the energy of the adsorbates (referenced to gas-phase O_2), E_{slab} is the energy of the clean slab, and N is the number of adsorbates.

The activation barrier (E_a) and reaction energy (ΔE) were calculated as:

$$E_a = E_{form,TS} - E_{form,IS}, \quad \Delta E = E_{form,FS} - E_{form,IS} \quad (2)$$

where $E_{form,IS}$, $E_{form,TS}$ and $E_{form,FS}$ are the formation energies of the initial state (IS), the transition state (TS) and the final state (FS), respectively.

The lateral O–O interaction energy (E_{int}) was defined by:

$$E_{int} = E_{adsorbate/slab} - (E_{adsorbate} + E_{slab}) - N \times E_O \quad (3)$$

where E_O is the adsorption energy of a single O* adatom at the f or h site.

3. Results and discussion

3.1 The adsorption of molecular O_2

The adsorption of an O_2 molecule on unstrained Pt(111) has been investigated extensively both experimentally[28–31] and theoretically.[10,11,32,33] Here, we take the three most energetically favorable adsorption configurations from the literature, namely, the top–bridge–top (tbt), top–fcc–bridge (tfb) and top–hcp–bridge (thb) configurations (Fig. 1b–d), which are named after their adsorption geometry. Other O_2 adsorption configurations that we tested are not as energetically favorable under strain, and they all end up as the aforementioned three configurations after geometry optimization (Fig. S1 and S2, ESI†). When assuming the tbt configuration (Fig. 1b), the O_2 molecule centers over a bridge (b) site with its axis parallel to the surface and each O atom locates near a top (t) site. In the tf(h)b configurations (Fig. 1c and d), the O_2 molecule spans over the f(h) site with two O atoms binding near the t and b site, respectively. As a result, in both configurations, O_2 tilts by about 10° relative to the surface, consistent with earlier works.[32,34] The b, t, f, and h sites are the stable adsorption sites of atomic O on the Pt(111) surface (Fig. 1a).

When no strain is applied, O_2 prefers to adsorb in the tbt configuration (E_{form} = −0.63 eV), while the O_2 adsorption is slightly weaker in the tfb configuration (E_{form} = −0.56 eV) and weaker still in the thb configuration (E_{form} = −0.48 eV), all agreeing well with the results of Qi *et al.*[10] and Kattel *et al.*[35]

However, strain exerts an important influence over the O_2 adsorption. Like in many previously published works for other systems,[2,36–38] in general, tensile strain strengthens adsorption whereas compressive strain weakens it, which has been well

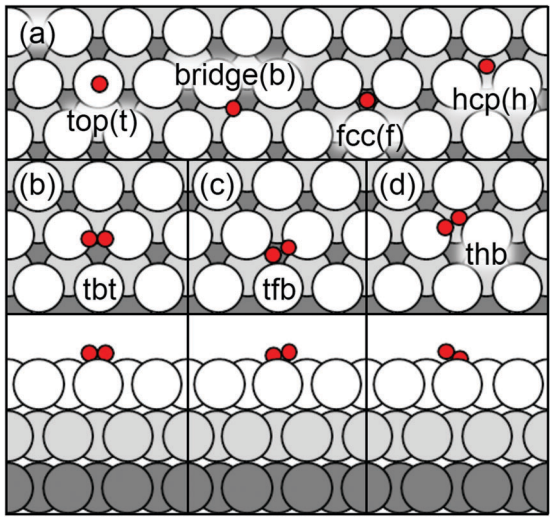

Fig. 1 Schematic illustration of adsorption sites for (a) atomic O and (b–d) molecular O_2 on Pt(111). The bottom three panels are the side view and the rest are the top view. Large circles represent Pt atoms and small red circles represent oxygen atoms.

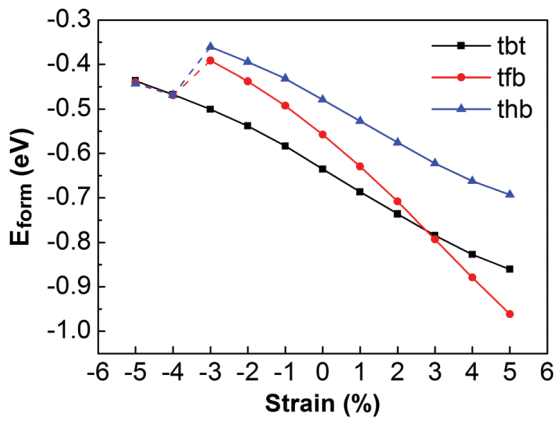

Fig. 2 Effect of strain on the adsorption energy (E_{ads}) of O_2 molecule on Pt(111). Solid and dashed lines are drawn as a guide to the eye. Dashed lines indicate the shift of O_2 from tfb and thb configurations to the tbt configuration when under over 3% or more compressive strain.

explained by the d-band center model. Within the considered strain range (±5%), the O_2 adsorption strength of all three configurations varies significantly by 0.3 to 0.6 eV (Fig. 2), which is much more significant than for the adsorption of O_2 on other metal surfaces like Cu(111) or Au(111).[37,39] Tensile strain also reduces the distance between the surface-bound O_2 molecule and the surface Pt atoms, *e.g.* the shortest d_{O-Pt} distances in the tfb configuration are 2.177 and 2.042 Å under 0 and 5% strain, respectively. For the bond length of O_2 (d_{O-O}), its change induced by strain varies among the configurations: d_{O-O} of a tbt O_2 barely gets affected, while the d_{O-O} values of tfb and thb O_2 molecules are stretched by tensile strain and shortened by compressive strain, with a changing rate of about 0.004 Å per 1% strain.

Subsequently, strain can change the order of their relative adsorption strength. When tensile strain goes beyond 3%, the most energetically favorable adsorption configuration changes from tbt to tfb (Fig. 2), which is in line with the result of Grabow *et al.*[18] wherein the preferred adsorption configuration changes from tbt to tfb under 4% strain, and the thb configuration always remains the weakest. Actually, the relative stability of tbt and tfb is reversed in some calculations for unstrained Pt(111).[11,12] We noticed that a rotation with a small barrier (0.11 eV on unstrained Pt(111)) can transform a tbt O_2 into the tfb configuration (Fig. S3 and Table S1, ESI†).

In addition, when compressive strain exceeds −3%, the tfb and thb configurations are no longer stable, and O_2 moves into the tbt configuration (dashed short lines in Fig. 2).

3.2 The dissociation of O_2

After adsorption, molecular O_2 tends to dissociate on Pt(111) when the temperature exceeds about 150 K. There are a number of O_2 dissociation pathways on Pt(111) that have been identified by computations.[10–13] The most representative two start from the tbt configuration but end as two O* adatoms at two neighboring f (pathway I in Fig. 3) or h sites (pathway II in Fig. 4). The two pathways were studied under three circumstances (0%, ±3% strain) and the corresponding energies and geometrical parameters of the key states (IS, TS, and FS) are listed in Tables 1 and 2.

For pathway I, on the unstrained surface, the tbt O_2 molecule rotates into the thb configuration, maintaining its molecular state with a slight bond elongation (Δd_{O-O} = 0.03 Å). Afterwards, the O–O bond begins to stretch with one O atom staying near the t site and the other O atom reaching out to the b site to form the TS (t–h–b, Fig. 3a). Finally, the two O atoms slip into the two respective neighboring f sites. The pathway

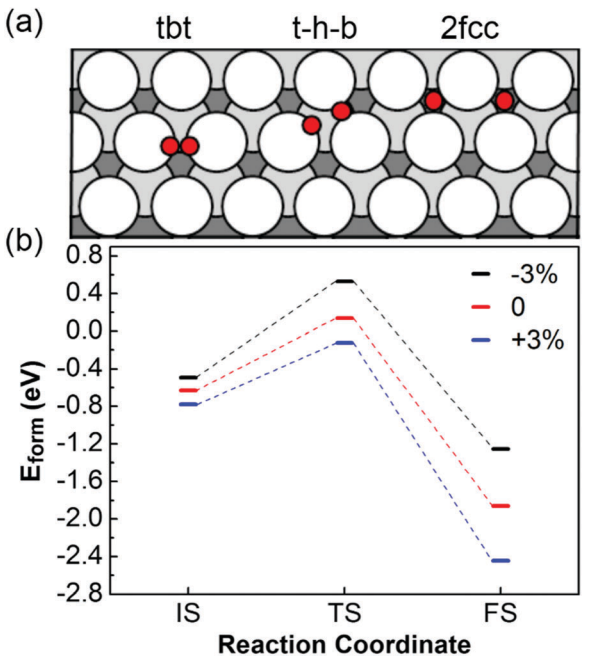

Fig. 3 O_2 dissociation pathway I on the strained Pt(111) surface. (a) Schematic illustration of the IS (tbt), TS (t–h–b) and FS (2fcc), and (b) key state energies.

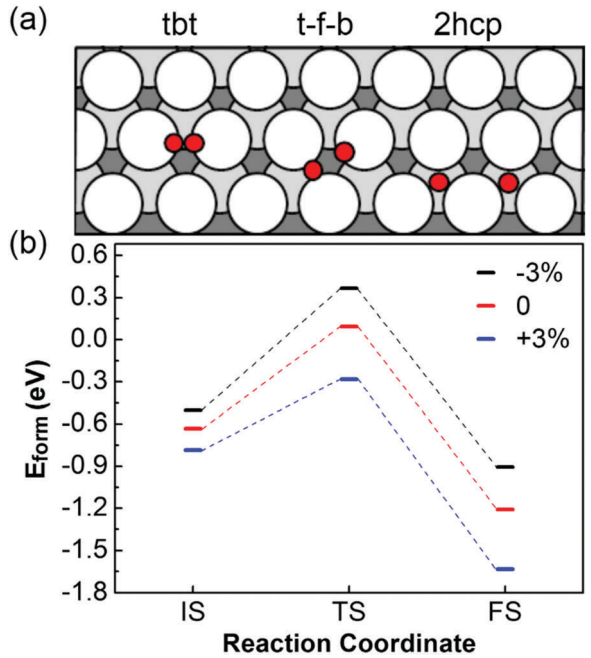

Fig. 4 O_2 dissociation pathway II on the strained Pt(111). (a) Schematic illustration of the IS (tbt), TS (t–f–b) and FS (2hcp), and (b) key state energies.

and barrier (E_a = 0.77 eV) agree well with the results of Xu *et al.*[6] (E_a = 0.77 eV) and Eichler *et al.*[40] (E_a = 0.72 eV).

Then, the same process was evaluated under ±3% strain. Consistent with the d-band theory, tensile strain stabilizes all the states along the dissociation pathway, and the activation energy (E_a) decreases slightly by 0.11 eV to 0.66 eV under 3% tensile strain (Table 1), which is caused by different degrees of stability enhancement for the IS and TS. In contrast, compressive strain exhibits the opposite influence but to a much bigger extent: E_a increases by 0.25 eV to 1.02 eV under −3% strain. This value is bigger than the result of Kattel *et al.*,[35] wherein the authors found that −3% strain would increase the E_a of O_2 dissociation by 0.14 eV. This difference may come from the different size of the model we use. The strain effects on dissociation pathway I are consistent with the results of Grabow *et al.*,[18] who reported that a +4% stain could decrease E_a by 0.06 eV and a −2% strain could increase E_a by 0.12 eV. However, the change of E_a under +4% stain is much smaller than the value we got under +3% strain, which is probably because the dissociation pathway under +4% stain is slightly different from ours, with a tfb IS instead of the tbt IS. Compressive strain beyond 2% results in a large change of energetics for O_2 dissociation for pathway I. The much bigger change in E_a under compressive strain is due to its greater destabilization effect on the TS. When 3% compressive strain is applied, the TS O–O distance increases evidently from 1.95 to 1.99 Å and the corresponding O–Pt distance increases from 1.90 to 2.08 Å, which leads to a large energy increase of about 0.4 eV for the TS. On the other hand, the IS (tbt) state is only changed slightly (0.14 eV variation in energy), thus E_a is much higher compared to the unstrained case. Apart from E_a, strain can also tune the reaction energy (ΔE) of O_2 dissociation (Table 1). Because of the much bigger change of the FS's E_{form}, tensile strain results in more exothermic dissociation with a smaller ΔE (more negative), while compressive strain results in a bigger ΔE (less negative), which is in line with the results of Kattel *et al.*[35] Considering E_a and ΔE, we can say that the dissociation of O_2 is thermodynamically and kinetically favored on the stretched Pt(111) surface, which is consistent with the results published by Grabow *et al.*[18]

In pathway II, unlike in pathway I, the IS tbt O_2 molecule rotates oppositely towards the neighboring f site rather than the h site, forming a different TS (t–f–b, Fig. 4a). Both bigger d_{O-O} values and smaller values of imaginary vibration frequency suggest a stronger interaction between O–O and the Pt atoms nearby, which differs substantially from the TS centering at the h site in pathway I (Table 1). Eventually, the two O atoms slip into their respective h sites. Strain essentially has the same effect on pathway II as on pathway I: +3% strain stabilizes the entire pathway and reduces E_a and ΔE by 0.22 eV and 0.28 eV, respectively, while −3% strain destabilizes the energetics and increases E_a and ΔE by 0.14 eV and 0.17 eV, respectively (Table 2). ΔE in pathway II are bigger than those in pathway I, which is because the FS in pathway II (2hcp O* atoms) is less stable than that in pathway I (2fcc O* atoms).

The change of energetics of the two pathways under strain suggests that the catalytic performance of the Pt(111) surface can be significantly (ΔE_a about 0.4 eV) tuned by a relatively small strain (about ±3%), either to be more active (tensile) or more inert (compressive) for O_2 dissociation. Strain makes pathway II more competitive kinetically by having much lower barriers than in pathway I, in spite of their close barriers when no strain is applied. However, in pathway II, the dissociated two O* atoms are at h sites, rather than at the more stable f sites, which will be eventually occupied *via* diffusion (Fig. S4 and S5, ESI†). It is also worth noting that d_{O-O} and the imaginary frequency of the TS do not show consistent trends with strain, which reflects the complex interactions between the TS O–O and the surface Pt atoms.

3.3 The adsorption of O* adatoms

Atomic O adsorption on Pt(111) has been widely investigated,[41–44] but the strain effects on adsorption induced

Table 1 Characteristic parameters of the O_2 dissociation pathway I

	d_{O-O} (Å)								
Strain (eV)	IS	TS	FS	Imaginary frequency (cm^{-1})	$E_{form,IS}$ (eV)	$E_{form,TS}$ (eV)	$E_{form,FS}$ (eV)	E_a (eV)	ΔE (eV)
−3	1.34	1.99	3.00	324.00	−0.49	0.53	−1.25	1.02	−0.76
0	1.34	1.95	2.98	334.86	−0.63	0.14	−1.86	0.77	−1.23
+3	1.35	1.92	3.01	328.57	−0.78	−0.12	−2.44	0.66	−1.66

Table 2 Characteristic parameters of the O_2 dissociation pathway II

Strain (eV)	d_{O-O} (Å) IS	TS	FS	Imaginary frequency (cm^{-1})	$E_{form,IS}$ (eV)	$E_{form,TS}$ (eV)	$E_{form,FS}$ (eV)	E_a (eV)	ΔE (eV)
−3	1.34	2.13	3.17	196.37	−0.49	0.37	−0.90	0.86	−0.41
0	1.34	2.15	3.09	187.55	−0.63	0.09	−1.21	0.72	−0.58
+3	1.35	2.16	3.02	119.65	−0.78	−0.28	−1.64	0.50	−0.86

surface buckling and the subsequent influences on the lateral O–O interaction energy have not been reported. In this section, we studied one, two, and three O* adatoms in different configurations on Pt(111) under −5% to 5% strain (Fig. 5a). For a single O* adatom, two three-fold stable O adsorption sites (the more stable f and less stable h sites) were considered. For two O* adatoms, in addition to the configurations right after the O_2 dissociation, namely, O* adatoms are located at the two first nearest neighboring f or h sites (denoted as 2O 1NN (fcc) and 2O 1NN (hcp), respectively), we also considered two O* adatoms located at the second nearest neighboring f sites (denoted as 2O 2NN). For three O* adatoms, the configuration of O atoms at the three first nearest neighboring f sites (denoted as 3O 1NN) was taken into consideration. We analyzed the formation energy (E_{form}), the lateral O–O interaction energy (E_{int}) and the Pt(111) surface buckling under strain conditions.

Surface geometric changes induced by O* adatoms have been observed previously, and they are always seen as the first step of Pt oxidation.[45–47] The surface Pt atoms may have lateral and/or vertical displacements during oxygen adsorption. The lateral displacements are in general negligible compared with the vertical ones, so we use the vertical displacement (ΔZ) of the Pt atom sandwiched or surrounded by O* adatoms to measure the surface buckling quantitatively (Fig. 5a, the side view panel is exaggerated for clearer illustration).

The O* adatom preferentially binds to the f site with an E_{form} of −1.03 eV, whereas the h site binding is 0.41 eV less stable on an unstrained Pt(111) surface, which is consistent with the previous DFT calculations.[6,44,48] Furthermore, the E_{form} values of 2O 1NN (fcc) (Fig. 5b, blue line), 2O 2NN (Fig. 5b, magenta line) and 3O 1NN (Fig. 5b, orange line) fall in between those of the f and h adsorption sites, as the repulsion among the O* adatoms reduces their adsorption strength. Thus, the order of

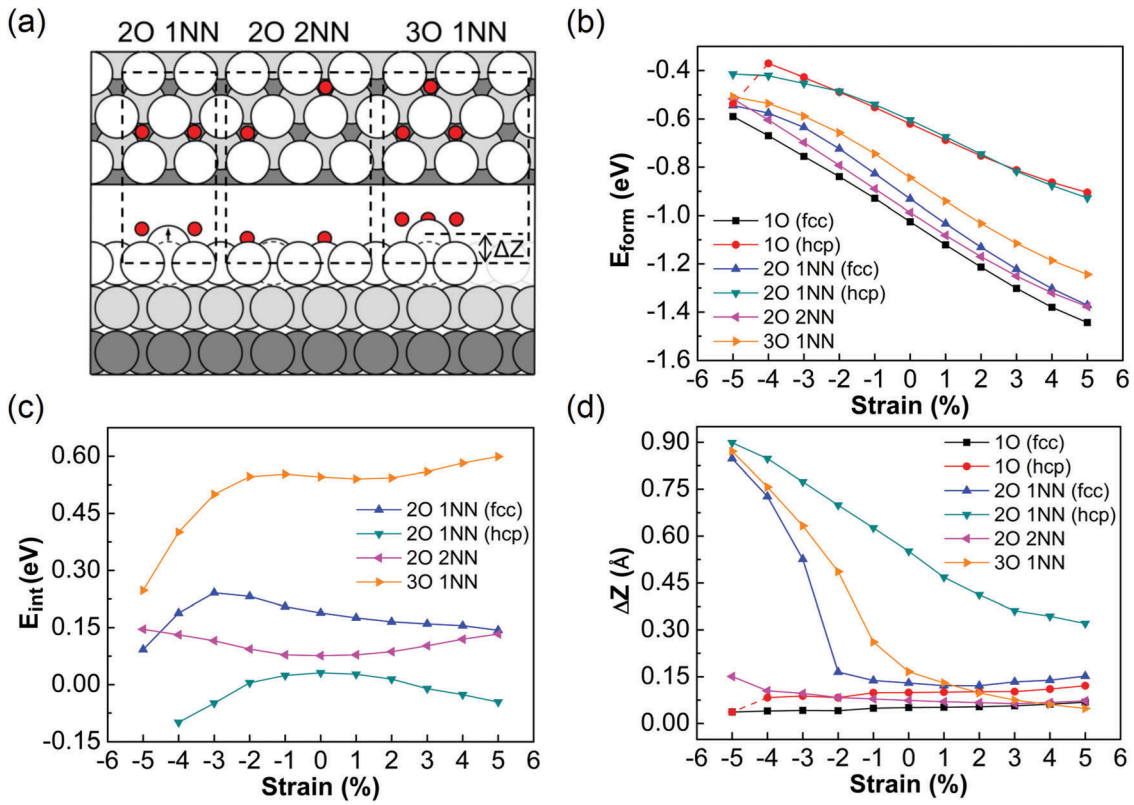

Fig. 5 Lateral interaction and surface buckling. (a) Adsorption configurations of O atoms on the Pt(111) surface, (b) effect of strain on the formation energy (E_{form}) of O atoms, (c) effect of strain on the lateral interaction energy (E_{int}) of O atoms, (d) effect of strain on the displacement of the specific Pt atom in the z direction (ΔZ). Solid lines in (a, b and c) are drawn as a guide to the eye. The dashed segments in (b and d) denote that the h site O atom slides to the f site under −5% strain.

adsorption strength in terms of E_{form} on the unstrained Pt(111) surface is 2O 2NN > 2O 1NN (fcc) > 3O 1NN > 2O 1NN (hcp) (Fig. 5b).

Within the considered strain range (±5%), 1O h exhibits the narrowest variation in E_{form} (ΔE_{form} about 0.5 eV), while 1O f presents a much wider variation range (ΔE_{form} about 0.9 eV). This suggests that strain is powerful in tuning the binding strength of O, especially for the most stable O adsorbing fcc site. At −5% strain, hcp is no longer stable for O adsorption, and it moves to an fcc like site (dashed line, Fig. 5b).

For multi-oxygen configurations, 2O 2NN shows the same strain response as 1O f adsorption, with its E_{form} nearly parallel to that of 1O f. This is because the O–O lateral repulsion at 2NN remains almost constant (about 0.1 eV) throughout the strain range (Fig. 5c, magenta line). For the other multi-oxygen configurations, however, the E_{form} show obvious non-linear changes when compressive strain goes beyond certain values (Fig. 5b, cyan line, orange line and blue line in the compressive strain region), which is because of the decrease of O–O repulsion in the same compressive strain range (Fig. 5c, cyan line, orange line and blue line in the compressive strain region). It is also worth noting that the E_{form} of 2O 1NN (hcp) (Fig. 5b, cyan line) almost overlaps with that of 1O at the h site (Fig. 5b, red line) when strain ranges from −3% to 5%. This means that the O–O lateral interaction is pretty small (Fig. 5c, cyan line), which is counterintuitive because the O–O distance here is close to that of 2O 1NN (fcc) and much smaller than that of 2O 2NN. These abnormal phenomena (the non-linear changes of E_{form} and E_{int} under compressive strain and the pretty small O–O lateral interaction for 2O 1NN (hcp)) all arise from the shift of the Pt atom's position, particularly in the z direction under strain conditions.

Fig. 5d shows that the buckling of the Pt atom in 2O 1NN (fcc) (Fig. 5d, blue line) and 3O 1NN (Fig. 5d, orange line) increases sharply from less than 0.25 Å at −2% and −1% strain up to about 0.85 Å under −5% strain, respectively. The buckled Pt atom leads to larger distances between O atoms (the O atoms do not sit exactly in the hollow sites anymore), which weaken the repulsive interaction. For 2O 1NN (hcp) (Fig. 5d, cyan line), the ΔZ of the O-sandwiched Pt atom is always larger than 0.3 Å in the entire strain range, so the obvious outward buckling of the Pt atom screens the O–O repulsion efficiently, sometimes it even turns the repulsion into slight attraction (Fig. 5c, cyan line). In contrast, the 1O and 2O 2NN adsorptions do not cause obvious surface buckling under the given strain range. Overall, when under compressive strain, the Pt(111) surface tends to reconstruct more easily, which probably helps oxidization, while tensile strain tends to enhance adsorption but not facilitate its oxidation.

4. Conclusion

In this study, we have systematically investigated the adsorption behaviors of O_2 and O* adatoms, as well as O_2 dissociation, on the Pt(111) surface under strain utilizing DFT calculations. We find that for molecular O_2 and atomic O, the change in formation energy (ΔE_{form}) caused by (±5%) strain is substantial: 0.3–0.6 eV for the former and 0.5–0.9 eV for the latter. The most favorable molecular adsorption site changes from tbt to tfb when tensile strain reaches over 3%. As for the dissociation of O_2, compressive strain hinders the process by increasing the barrier (E_a) and reaction energy (ΔE) while tensile strain does the opposite. Significant ΔE_a (0.36 eV) is induced by strains of −3% and +3% for both dissociation pathways, and the ΔE is changed by 0.9 eV and 0.45 eV for the two dissociation pathways, respectively. The lateral repulsive interactions between O–O are much less sensitive to strain than the O_2 and O adsorptions. Yet, the geometric changes of Pt(111) induced by compressive strain of two or three O* adatoms at 1NN configurations are significant, which leads to evident surface buckling (*e.g.* ΔZ of the most buckling Pt atom is over 0.50 Å under −3% strain for 2O 1NN), which is also the cause of the non-linear responses of E_{form} and E_{int} to strain.

All the behaviors of atomic and molecular oxygen on Pt(111) suggest that strain can serve as a handle to widely tune the thermodynamic and kinetic properties of the adsorbates, and it can greatly influence the catalyst surface structure during oxidation reactions, particularly when the catalysts are nanoparticles or heterostructure materials, where strain exists natively.

The strain effects on the behaviors of O_2/O over the Pt(111) surface have been discussed in detail, however, if O_2-related real reactions, such as the ORR, are considered, the impact of strain on the whole reaction requires similar investigations into each elementary reaction step involved, which will be our future work.

Conflicts of interest

There are no conflicts to declare.

Acknowledgements

This work was supported by the National Natural Science Foundation of China (No. 51320105014, 51621063, 21477096). The authors would like to thank Mr. Fuzhu Liu from Xi'an Jiaotong University for useful discussions.

References

1 J. Wu, P. Li, Y. T. Pan, S. Warren, X. Yin and H. Yang, *Chem. Soc. Rev.*, 2012, **41**, 8066–8074.
2 B. Yildiz, *MRS Bull.*, 2014, **39**, 147–156.
3 S. Yang, F. Liu, C. Wu and S. Yang, *Small*, 2016, **12**, 4028–4047.
4 M. J. Janik, C. D. Taylor and M. Neurock, *J. Electrochem. Soc.*, 2009, **156**, B126–B135.
5 P. Strasser, S. Koh, T. Anniyev, J. Greeley, K. More, C. Yu, Z. Liu, S. Kaya, D. Nordlund, H. Ogasawara, M. F. Toney and A. Nilsson, *Nat. Chem.*, 2010, **2**, 454–460.
6 Y. Xu, A. V. Ruban and M. Mavrikakis, *J. Am. Chem. Soc.*, 2004, **126**, 4717–4725.

7 M. Li, Z. Zhao, T. Cheng, A. Fortunelli, C. Y. Chen, R. Yu, Q. Zhang, L. Gu, B. V. Merinov, Z. Lin, E. Zhu, T. Yu, Q. Jia, J. Guo, L. Zhang, W. A. Goddard, Y. Huang and X. Duan, *Science*, 2016, **354**, 1414–1419.
8 J. Wu, L. Qi, H. You, A. Gross, J. Li and H. Yang, *J. Am. Chem. Soc.*, 2012, **134**, 11880–11883.
9 S. P. Devarajan, J. A. Hinojosa and J. F. Weaver, *Surf. Sci.*, 2008, **602**, 3116–3124.
10 L. Qi, J. Yu and J. Li, *J. Chem. Phys.*, 2006, **125**, 054701.
11 J. S. McEwen, J. M. Bray, C. Wu and W. F. Schneider, *Phys. Chem. Chem. Phys.*, 2012, **14**, 16677–16685.
12 Z. Yang, J. Wang and X. Yu, *Phys. Lett. A*, 2010, **374**, 4713–4717.
13 B. Shan, N. Kapur, J. Hyun, L. Wang, J. B. Nicholas and K. Cho, *J. Phys. Chem. C*, 2009, **113**, 710–715.
14 D. C. Ford, Y. Xu and M. Mavrikakis, *Surf. Sci.*, 2005, **587**, 159–174.
15 D. Fantauzzi, J. E. Mueller, L. Sabo, A. C. Van Duin and T. Jacob, *ChemPhysChem*, 2015, **16**, 2797–2802.
16 E. F. Holby, J. Greeley and D. Morgan, *J. Phys. Chem. C*, 2012, **116**, 9942–9946.
17 D. J. Miller, H. Öberg, S. Kaya, H. Sanchez Casalongue, D. Friebel, T. Anniyev, H. Ogasawara, H. Bluhm, L. G. M. Pettersson and A. Nilsson, *Phys. Rev. Lett.*, 2011, **107**, 195502.
18 L. Grabow, Y. Xu and M. Mavrikakis, *Phys. Chem. Chem. Phys.*, 2006, **8**, 3369–3374.
19 B. Delley, *J. Chem. Phys.*, 2000, **113**, 7756–7764.
20 B. Delley, *J. Chem. Phys.*, 1990, **92**, 508–517.
21 J. P. Perdew, J. A. Chevary, S. H. Vosko, K. A. Jackson, M. R. Pederson, D. J. Singh and C. Fiolhais, *Phys. Rev. B: Condens. Matter Mater. Phys.*, 1992, **46**, 6671–6687.
22 J. A. White and D. M. Bird, *Phys. Rev. B: Condens. Matter Mater. Phys.*, 1994, **50**, 4954–4957.
23 B. Delley, *Phys. Rev. B: Condens. Matter Mater. Phys.*, 2002, **66**, 155125.
24 M. Lischka, C. Mosch and A. Groß, *Electrochim. Acta*, 2007, **52**, 2219–2228.
25 D. Lide, *CRC Handbook of Chemistry and Physics*, CRC Press, Boca Raton, FL, 2004.
26 T. A. Halgren and W. N. Lipscomb, *Chem. Phys. Lett.*, 1977, **49**, 225–232.
27 N. Govind, M. Petersen, G. Fitzgerald, D. King-Smith and J. Andzelm, *Comput. Mater. Sci.*, 2003, **28**, 250–258.
28 H. Steininger, S. Lehwald and H. Ibach, *Surf. Sci.*, 1982, **123**, 1–17.
29 B. C. Stipe, M. A. Rezaei, W. Ho, S. Gao, M. Persson and B. I. Lundqvist, *Phys. Rev. Lett.*, 1997, **78**, 4410–4413.
30 P. D. Nolan, B. R. Lutz, P. L. Tanaka, J. E. Davis and C. B. Mullins, *J. Chem. Phys.*, 1999, **111**, 3696–3704.
31 W. Wurth, J. Stöhr, P. Feulner, X. Pan, K. R. Bauchspiess, Y. Baba, E. Hudel, G. Rocker and D. Menzel, *Phys. Rev. Lett.*, 1990, **65**, 2426–2429.
32 A. Eichler and J. Hafner, *Phys. Rev. Lett.*, 1997, **79**, 4481–4484.
33 R. B. Getman, W. F. Schneider, A. D. Smeltz, W. N. Delgass and F. H. Ribeiro, *Phys. Rev. Lett.*, 2009, **102**, 076101.
34 M. L. Bocquet, J. Cerdà and P. Sautet, *Phys. Rev. B: Condens. Matter Mater. Phys.*, 1999, **59**, 15437–15445.
35 S. Kattel and G. Wang, *J. Chem. Phys.*, 2014, **141**, 124713.
36 M. Mavrikakis, B. Hammer and J. K. Nørskov, *Phys. Rev. Lett.*, 1998, **81**, 2819–2822.
37 Y. Xu and M. Mavrikakis, *Surf. Sci.*, 2001, **494**, 131–144.
38 X. Wang, M. Khafizov and I. Szlufarska, *J. Nucl. Mater.*, 2014, **445**, 1–6.
39 Y. Xu and M. Mavrikakis, *J. Phys. Chem. B*, 2003, **107**, 9298–9307.
40 A. Eichler, F. Mittendorfer and J. Hafner, *Phys. Rev. B: Condens. Matter Mater. Phys.*, 2000, **62**, 4744–4755.
41 U. Starke, N. Materer, A. Barbieri, R. Döll, K. Heinz, M. A. Van Hove and G. A. Somorjai, *Surf. Sci.*, 1993, **287–288**, 432–437.
42 N. Materer, U. Starke, A. Barbieri, R. Döll, K. Heinz, M. A. Van Hove and G. A. Somorjai, *Surf. Sci.*, 1995, **325**, 207–222.
43 H. Tang, A. Van der Ven and B. L. Trout, *Phys. Rev. B: Condens. Matter Mater. Phys.*, 2004, **70**, 2199–2208.
44 P. J. Feibelman, S. Esch and T. Michely, *Phys. Rev. Lett.*, 1996, **77**, 2257–2260.
45 M. J. Eslamibidgoli and M. H. Eikerling, *Electrocatalysis*, 2016, **7**, 345–354.
46 D. Miller, H. Sanchez Casalongue, H. Bluhm, H. Ogasawara, A. Nilsson and S. Kaya, *J. Am. Chem. Soc.*, 2014, **136**, 6340–6347.
47 J. M. Hawkins, J. F. Weaver and A. Asthagiri, *Phys. Rev. B: Condens. Matter Mater. Phys.*, 2009, **79**, 125434.
48 R. B. Getman, Y. Xu and W. F. Schneider, *J. Phys. Chem. C*, 2008, **112**, 9559–9572.